Materials Research. 2025; 28:e20240444
DOI: https://doi.org/10.1590/1980-5373-MR-2024-0444

Silica Gel Functionalized with Cu, Ag and ZnO as an Absorbent System in Active Packaging

Zaira Nicole Silva Guido*[a,b], *Marcus Vinicius Braum*[c], *Natália Morelli Possolli*[a], *Rafaella De Bonna*[a], *Elídio Angioletto*[a], *Matheus Vinicius Gregory Zimmermann*[a]

[a]*Universidade do Extremo Sul Catarinense (UNESC), Programa de Pós-Graduação em Ciência e Engenharia de Materiais, Criciúma, SC, Brasil.*
[b]*Instituto Senai de Inovação em Materiais Avançados e Nanocompósitos, São Bernardo do Campo, SP, Brasil.*
[c]*Prometeon Tyre Group, Santo André, SP, Brasil.*

Received: September 30, 2024; Revised: December 31, 2024; Accepted: January 30, 2025

Silica gel was synthesized from rice husk silicate, a sustainable feedstock, and functionalized with Ag, Cu, and ZnO nanoparticles to evaluate the liquid absorption capacity of these nanocomposites and their potential use in active packaging. From a two-level full factorial experiment, where pH, silicate modulus and SiO_2 concentration were tested, silicas with varied surface areas (250-750 m^2/g) and pore volume (0.4-1.0 cm^3/g) were obtained. The silica with the highest porosity (1.0 cm^3/g) was synthesized from a solution containing silicate with a modulus of 2.0 and a SiO_2 concentration of 20 g/L, by acidification to pH 6. The product obtained showed the highest absorption of water and simulated body fluid (190%) and was chosen as the matrix for functionalization with nanoparticles produced from chemical reduction (Cu, Ag) and precipitation (ZnO) methods. The incorporation of ZnO nanoparticles into the silica matrix had an additional contribution to liquid absorption, at a rate of 0.04%/ppm.

Keywords: *silica gel, functionalization, active packaging, liquid absorption, rice husk ash, nanomaterials.*

1. Introduction

Currently, Brazil produces an average of 11 million tons of rice per year, with 20% of this production concentrated in the extreme south region of the country, totaling around 2,500 km^2 of planted area[1]. As a result of this agricultural activity, about 500,000 tons of rice husk are disposed annually in large, open-air deposits in the region. This results in the emission of atmospheric pollutants, such as greenhouse gases (CO_2, CH_4) and ash, deriving from spontaneous combustion, as well as the generation of leachate that contaminates the soil and local water sources[2]. Therefore, industrial initiatives that make rice husk a valued raw material, such as the production of synthetic amorphous silicas from rice husk ash, could encourage its environmentally correct disposal, in a circular economy concept, and help to decarbonize the agri-food sector.

Active packaging systems have been a strategy to minimize waste of fresh meat foods, acting to absorb exudate and inhibit microbial growth, protein oxidation and lipid oxidation, extending the food shelf-life[3,4]. Thus, technologies involving moisture control, such as desiccants and absorbents, are often used in packaging of fresh meats, fruits and vegetables to reduce water activity, while antimicrobial substances incorporated into packaging inhibit or eliminate spoilage and pathogenic microorganisms[5]. A variety of materials have been considered for use in absorbent pads, such as wood fluff pulp, super-absorbent polymers, nanofibers, super-absorbent aerogels, zeolites, silica gel, etc[6-8]. Similarly, many antimicrobial agents have been used or tested for meat preservation, such as synthetic preservatives[9,10], essential oils[11], cationic polymers[7], nanoparticles[5,12], among others. However, many of these preservatives have adverse effects and shortcomings, for instance, synthetic preservatives may cause cancer, degenerative diseases and poisoning[9], essential oils are strongly volatile and can be irritating[7], while many natural antimicrobials can alter some sensorial characteristics of meat[3]. Currently, the use of composite materials containing nanoparticles in active packaging systems has become increasingly widespread[12].

The non-toxic and amorphous structure of the SiO_2-based desiccants[13] allows its application in research focused on the area of active and intelligent packaging[14,15] as an alternative to extend the shelf life of food, maintaining its sensorial characteristics of appearance, aroma, consistency, texture, and flavor[3]. The action of silica gel in humidity control applied to active packaging can occur through the adsorption of relative humidity from the air and/or the absorption of fluids exuded by the food, and the effect of silica's morphological characteristics (surface area, volume and pore size distribution) on the adsorption capacity of atmospheric moisture are the main parameters, already extensively covered in the literature[16,17]. However, it is still necessary to further research regarding the impacts of such

*e-mail: matheus.vgz@gmail.com

characteristics on the absorption and retention of different types of liquids, as well as the presence of functionalized metallic nanoparticles in the silica matrix.

Regarding antimicrobial activity, the use of nanomaterials, mainly in the form of nanoparticles and metal oxides, has grown in recent years[18,19]. The great advantage of using antimicrobial agents in active packaging is that it allows for a reduction in the preservative content in food, a measure that satisfies a specific market niche which seeks minimally processed foods with minimal levels of additives in their composition[20]. In the context of active packaging production, among the recent alternatives for preserving fresh food, nanoparticles of metals and metal oxides supported on a silica gel matrix stand out, which can be used in absorbent pads, thus managing to associate antimicrobial activity with high moisture adsorption capacity[5]. The antimicrobial effect of these metallic nanoparticles may be linked with the generation of hydrogen peroxide[21], resulting either in damage to the cell membrane and DNA[16], or in the interaction with enzymes from thiol groups[17].

The production of functionalized silica gel from rice husk silicate, for use in active packaging for meat, could be an opportunity to stimulate the use of rice husk, decarbonizing agricultural production and, simultaneously, reducing the carbon footprint of the meat processing industry, since silica produced from rice husk has a much lower carbon footprint than materials traditionally used as absorbents in active packaging for meat[22]. Considering this, the aim of this work is to preliminary study the water and simulated body fluid (SBF) retention capacity of silica gels (obtained from rice husk silicate) with different morphologies, through variations in the synthesis conditions, as well as functionalization with metallic nanoparticles.

2. Experimental Procedures

2.1. Materials

The sodium silicate solution produced from RHA (density = 1.183 g/cm^3, at 20 °C), used for the synthesis of silica gel, was supplied by the company Oryzasil Sílicas Naturais Ltda., Itaqui-RS/Brazil. The other reagents used, all in analytical grade, were sulfuric acid 95-97% (Merck), nitric acid 65% (Neon), ammonium hydroxide (Dinâmica Química Contemporânea Ltda), copper II acetate (Dinâmica Química Contemporânea Ltda), ascorbic acid (Neon), silver acetate (Plat-Lab), sodium hydroxide (Neon) and zinc nitrate hexahydrate (Neon). The simulated body fluid (SBF) was prepared according to the method described by Kokubo and Takadama[23] and ISO/FDIS 23317:2007.

2.2. Characterization of sodium silicate

The %SiO_2 and %(Na_2O + K_2O) were determined using the ISO 1690:1976[24] and ISO 1692:1976[25] methods, respectively. Initially, approximately 5 mL of silicate was added to a previously tared 125 mL Erlenmeyer flask and the mass of silicate (m_{S1}) was determined. The sample volume was then adjusted to a final volume of 50 mL with distilled water and the solution was titrated until pH 7.00 with a standard solution of 0.5 M H_2SO_4, under vigorous stirring. The total volume of acid added (Vac) was finally used to calculate the total content of Na_2O and K_2O, according to Equation 1, where M is the acid concentration:

$$\%(Na_2O + K_2O) = \frac{V_{ac} \times M \times 62}{1000 \times m_{s1}} \times 100 \quad (1)$$

Next, around 5 mL of silicate was added to a 125 mL Erlenmeyer flask. Then, 20 mL of distilled water was added and, under vigorous stirring, 3 mL of concentrated HCl. The solution was stirred for 5 min and then placed in an oven at 105 °C until all the water evaporated. After the solution cooled down, another 3 mL of concentrated HCl and 10 mL of distilled water were added. The Erlenmeyer flask was then placed in a water bath for 5 minutes under stirring and then the solution was filtered and the solid was washed with water at 40-50 °C until the measured conductivity of the filtrate was less than 10 µS/cm. Then, the filter paper containing the solid was dried in an oven for 2h at 105 °C, transferred to a previously calcined and tared crucible (m_{c1}), and taken to the muffle furnace to calcine at 900 °C until constant mass (m_{c2}) was achieved. The SiO_2 content was then calculated from Equation 2:

$$\%SiO_2 = \frac{m_{c2} - m_{c1}}{m_{s2}} \times 100 \quad (2)$$

Metallic contaminants were quantified by ICP-OES scanning (Inductively Coupled Plasma Optical Emission Spectroscopy), using Agilent Technologies equipment, model 720.

Another important characteristic of the silicate is the modulus or mass ratio (Wr), defined as the relationship between the mass percentages of SiO_2 (12.11%) and sodium and potassium oxides (4.73%) present in the sample, as indicated in Table 1. In this study, silicates of three different modulus were used: Wr = 2.56 (original sample), 2.0 and 1.50, the last two being obtained from the addition of 8.55 g and 21.57 g of sodium hydroxide to 500 g of original sample, respectively.

2.3. Silica gel synthesis

To obtain silica gels of different surface areas and pore morphologies, a full factorial experimental design (DOE) of 3 factors at 2 levels with a central point (CP) was applied. The factors chosen were the silicate modulus (Wr), the SiO_2 concentration and the final pH, with levels varying as indicated

Table 1. Full factorial experiment matrix with 2 levels and 3 input factors (silicate modulus, SiO_2 concentration and final pH) for evaluating the effect of synthesis parameters on the morphological characteristics of silica gel.

Test	Wr	[SiO_2]	pH
	—	g/L	—
R1	2.56	30	8
R2	1.50	30	4
R3	1.50	10	4
R4	2.56	10	4
R5	1.50	10	8
R6	2.56	10	8
R7	2.56	30	4
R8	1.50	30	8
CP	2.00	20	6

in Table 1. The control factors that were kept fixed were the concentration of sulfuric acid, the precipitation temperature, and the time of precipitation. Except for CP, performed in duplicate, all other syntheses were performed only once.

Procedure: To a 1,000 mL beaker, 600 mL of a previously prepared sodium silicate solution, with the required modulus and concentration of silicon dioxide, were added. After confirming that the temperature of the silicate solution was within the range of 25 ± 2 °C, the sulfuric acid solution (1.070 g/cm^3) was added drop by drop, under vigorous stirring at a constant rate, in order to reach the final pH in 60 ± 5 min. After adding the acid, the reaction mixture was kept under stirring for another 60 min, and then placed in an oven at 105 °C for 24 h to evaporate. The hydrogel obtained was then fragmented, suspended in 100 mL of distilled water preheated to 40 °C, filtered through filter paper and washed in successive steps with 2.5 L of water at 40 °C to remove sodium sulfate. The washed silica was dried again at 105 °C for 24 h and stored in a desiccator[26-28].

2.4. Synthesis of metallic nanoparticles for functionalization of silica gel

The synthesis of ZnO-Silica proceeded via the precipitation method[29]. Initially, 5 g of silica and 50 mL of deionized water were added to a 250 mL flat-bottom flask. Then, 1.0 mL of 0.005 M zinc nitrate solution and, subsequently, 10 mL of 0.1 M NaOH solution were added to the suspension, drop by drop, under magnetic stirring. The temperature of the mixture was raised to 60 °C and kept under stirring for 1 h. After filtering and washing the precipitate, it was subjected to calcination at 400 °C for 1 h. The ZnO-Silica obtained was preserved in a desiccator.

Silica gels functionalized with Cu (Cu-Silica) were synthesized by the chemical reduction method[30,31]. In a flat-bottom flask, 5 g of silica gel and 50 mL of deionized water were added. Then, 15 mL of 5% NH_4OH were added to the suspension, drop by drop and under magnetic stirring, followed by 1.0 mL of 0.005 M copper (II) acetate solution. After the temperature was raised to 80 °C, 1.7 mL of a 0.004 M ascorbic acid solution was added dropwise to the mixture, keeping it under stirring for 12 h. After filtering and washing, the precipitate was dried in an oven at 105 °C for 24 h and stored in a desiccator.

The preparation of Ag-Silica was also conducted according to the chemical reduction method[31,32]. Initially, 5 g of silica gel and 50 mL of deionized water were mixed in a flat-bottom flask. Under magnetic stirring, 1.1 mL of 0.1 M NaOH solution was then added and, subsequently, 15 mL of 5% NH_4OH. Soon after, 1.0 mL of 0.005 M silver acetate solution was added drop by drop and left to stir for 30 min, and the mixture was then neutralized with concentrated HNO_3. After filtration and washing, the precipitate was dried in an oven at 105 °C for 24 h and stored in a desiccator. Figure 1 presents the flowchart with the main steps of the methodology used in this work.

2.5. Characterization

2.5.1. Assessment of surface area and morphology

The morphological characteristics of the silica gel before and after functionalization with metallic nanoparticles (NPs) were determined from nitrogen adsorption/desorption isotherms at 77 K in a Microtrac nitrogen surface area and pore size distribution (PSD) analyzer (BELSORP-mini II). The surface area was determined by the BET method[33]. For predominantly mesoporous samples (pore size between

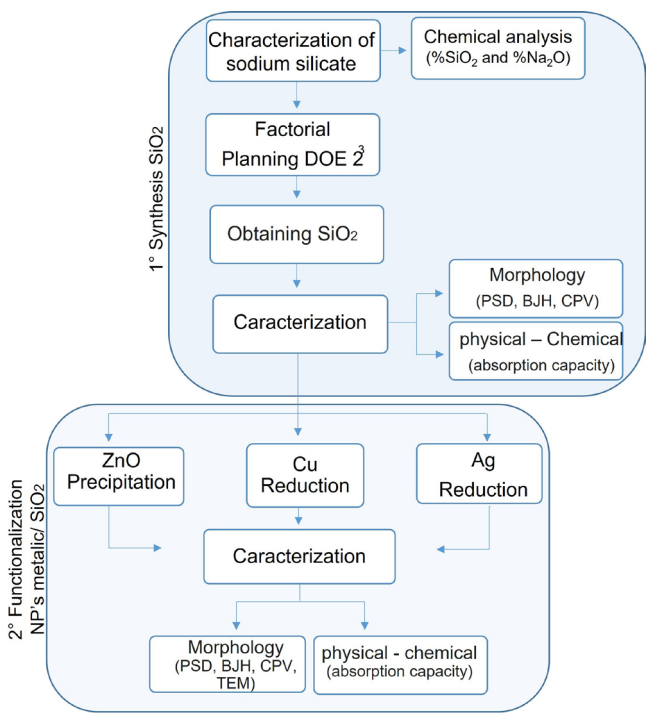

Figure 1. Flowchart with the main steps of the methodology used in this work.

2 and 50 nm), the PSD curves were obtained from the desorption isotherms, using the BJH method[34]. In the case of predominantly microporous silicas (pores of up to 2 nm), the PSD curves were obtained from the treatment of adsorption isotherms, using the MP method[35]. In all tests, samples were first degassed for 3 h at 300 °C under N_2 flow.

2.5.2. Assessment of liquid absorption and retention capacity

The assessment of the water absorption capacity and SBF by the silica samples before and after being functionalized with metallic NP's was carried out using the methodology proposed by Schaller and collaborators[36], where, after drying the silica at 105 °C for 12 h, approximately 1 g of sample was weighed (with a minimum precision of 1 mg) into a previously tared Falcon tube. Then, 15 mL of the test liquid was added and left to rest for 5 h, before centrifuging the suspension at 3,400 rpm for 20 min. Next, the unabsorbed amount of liquid was carefully removed, and the tube was weighed again. The maximum liquid retention capacity was obtained by the weight difference between the drained centrifuged sample and the dried sample.

2.5.3. Morphological assessment by transmission electron microscopy (TEM)

Sample preparation for TEM analyses involved the deagglomeration and dispersion of silica gel before and after functionalization with metallic nanoparticles through the application of ultrasonic energy in a Sonics sonicator (Vibra-Cell). In a beaker, 1.25 g of silica was added to 15 mL of absolute ethanol. The sonication of the samples proceeded with the introduction of the titanium tip to a depth of 19 mm and the application of an acoustic power of 32 W, pulsed at 80%, for 15 min. An ice bath was used around the beaker containing the suspension to avoid overheating the sample. The sonicated samples were left to rest for 24 h. Afterwards, an aliquot of the dispersion supernatant was collected, and 0.05 mL was added to a 5 mL beaker containing 0.5 mL of absolute ethanol. The suspension was then sonicated for 1 min in an ultrasonic bath and, shortly after, copper sample holders coated with Formvar® carbon film were immersed in 1 drop of suspension and left to dry for 12 h. After drying the sample holders' images of both the pure silica gel (matrix) and the silica gel functionalized with metallic nanoparticles were obtained from a JEOL transmission electron microscope (JEM-1011), operating with an acceleration potential of 80 kV.

2.5.4. Determination of nanoparticle content in silica samples

To quantify the metallic nanoparticles present in silica gel, the samples were prepared according to the EPA 3051A method and analyzed by ICP-OES according to the SMEWW 3120 B and EPA 6010C methods. The EPA 3051A preparation method consists of microwave-assisted acid digestion using nitric acid (HNO_3) and hydrochloric acid (HCl). However, since this method is not intended to perform total sample decomposition, extracted analyte concentrations may not reflect the total sample content. On the other hand, methods like SMEWW 3120 B and EPA 6010C describe the determination of trace elements in aqueous solution. A standard aerosol is generated in a suitable nebulizer and spray chamber and is injected into the plasma at temperatures of 6,000 to 8,000 K. The resulting ionization of a high percentage of atoms produces ion emission spectra that was analyzed using a monochromator to examine the wavelengths of the emission spectra. The method also lists recommended analytical wavelengths and estimated instrumental detection limits.

3. Results and Discussion

3.1. Sodium silicate composition

Knowing the chemical composition of the sodium silicate used is essential, both for controlling the silica gel synthesis reaction and for verifying the suitability of the raw material in terms of the presence and levels of metallic contaminants. Table 2 shows the values for the compositional analysis of sodium silicate. The majority of contaminants present came from agricultural waste itself, but the high mercury content stands out, with 2 mg/L being found in the sample analyzed. In this case, the source of contamination was probably the sodium hydroxide used to produce sodium silicate in industrial scale.

3.2. Surface area and pore morphology of silica gel

Firstly, the influence of silica gel processing parameters on morphology and sorption capacity was evaluated. In addition to being widely used to determine the BET surface area and PSD of porous solids, measuring adsorption at the gas/solid interface is also fundamental for understanding these materials' nature and surface behavior. Adsorption isotherms can show different characteristic shapes, can be divided into eight groups according to an extended IUPAC (International Union of Pure and Applied Chemistry)[37]

Table 2. Chemical composition of sodium silicate produced from rice husk ash.

Composition (%)		Contaminants (mg/L)							
SiO_2	12.11	As	0.044	Se	<1.00	Ca	15.60	Mn	0.167
		Pb	0.259	Al	1.580	Co	0.147	Mo	0.095
		S	1.891	Ba	<1.00	Cu	0.105	Ni	0.742
Na_2O+K_2O	4.73	Fe	0.273	Be	<0.50	Cr	<1.00	Ti	0.137
		P	60.52	Bi	1.369	Sn	1.200	V	0.063
		Hg	2.040	B	0.556	Mg	1.180	Zn	1.250

classification and provide important preliminary information about the structure of the adsorbent pores, allowing the choice of the most appropriate analysis method to be used in each case[37,38].

Figure 2 presents the N_2 adsorption and desorption isotherms at 77 K of the silica gels synthesized in this study. According to the IUPAC[37] classification, in Figure 2a, it is evident that samples R1, R5, R6, R8 and CP, acidified to a higher final pH (6 – 8), present Type IV isotherms and H1 hysteresis loop, typical characteristics of materials with a structure of cylindrical pores ranging in size between 2 and 50 nm (mesopores).

The isotherms of samples R2, R3, R4 and R7, synthesized at pH = 4 and presented in Figure 2b, showed a Type 1 format, typical of predominantly microporous solids (pores ≤ 2 nm). However, these isotherms also showed small H4 hysteresis loops, indicating the presence of narrow slit-like mesopores. Therefore, based on the analysis above, the BJH method was used to obtain the PSD curves for samples R1, R5, R6, R8 and CP (Figure 3a), while for samples R2, R3, R4 and R7 the MP method was applied (Figure 3b).

From the application of the BET, BJH and MP methods in specific regions of the adsorption/desorption isotherms, the BET surface area (S_{BET}), BET constant (C_{BET}), pore diameter at the distribution peak (d_p), and total volume of pores (V_p) of silica gels produced under different synthesis conditions were obtained, which are shown in Table 3. The results of the PSD analysis confirm the preliminary assessment carried out based on the isotherms' classification, since the samples considered microporous (R2, R3, R4 and R7) presented $d_p \leq 2$ nm and the samples considered predominantly mesoporous (R1, R5, R6, R8 and CP) showed d_p in the range of 2 to 50 nm. Furthermore, microporous samples exhibited a surface area of 742 ± 14 m^2/g, approximately 2.5 times larger, and a pore volume of 0.49 ± 0.05 cm^3/g, on average 1.7 times smaller than predominantly mesoporous silicas. It is also observed that after 80 days the characteristics of microporous silicas, on average, did not change significantly, while the mesoporous silicas experienced an average reduction of 19 m^2/g in surface area. This change may be the result of a process known as Ostwald ripening, in which small particles dissolve and redeposit at the junction region between larger particles (necks), due to the greater solubility of convex surfaces (higher surface energy). The higher final conductivity of the washing water of mesoporous silicas (113 ± 32 µS/cm) compared to microporous silicas (6.7 ± 1.8 µS/cm) indicates a much larger remaining amount of sodium sulfate in them, which can also have contributed to the accelerated aging of mesoporous samples[39].

The effect of varying reaction conditions on the silica gel's morphological characteristics can be better assessed

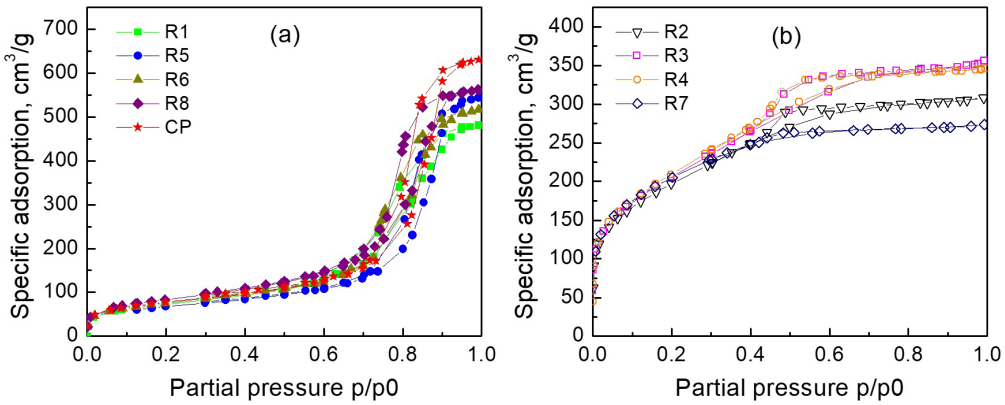

Figure 2. Nitrogen adsorption/desorption isotherms at 77 K for silica gels synthesized at (a) pH = 6 to 8 and (b) pH = 4.

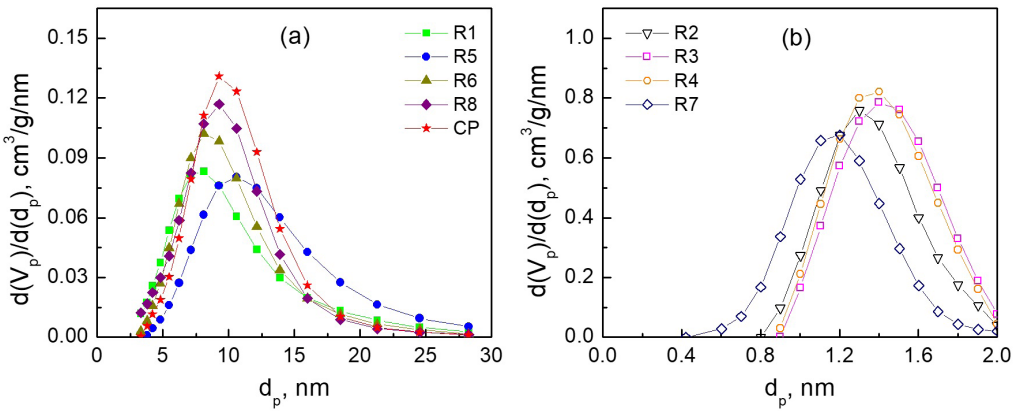

Figure 3. Pore size distributions (PSD) for: (a) mesoporous silica samples, using BJH method (desorption branch), and (b) microporous silica samples, using MP method.

Table 3. Characteristics of silica gel obtained from sodium silicate from rice husk under different synthesis conditions, immediately after analysis and after stabilization.

Sample	24 h after synthesis				80 days after synthesis			
	S_{BET}	C_{BET}	d_p	V_p	S_{BET}	C_{BET}	d_p	V_p
	m^2/g	—	nm	cm^3/g	m^2/g	—	nm	cm^3/g
R1	289	93	8.1	0.746	266	99	8.1	0.744
R2	722	101	1.3	0.481	715	98	1.3	0.476
R3	742	88	1.4	0.543	751	84	1.4	0.550
R4	754	88	1.4	0.528	765	84	1.4	0.534
R5	260	112	10.6	0.868	244	107	10.6	0.841
R6	295	108	8.1	0.802	276	103	8.1	0.799
R7	750	121	1.2	0.425	740	117	1.2	0.423
R8	331	95	9.2	0.875	305	99	9.2	0.870
CP(1)	323	99	9.2	0.944	302	103	10.6	0.946
CP(2)	292	102	10.6	0.954	282	104	10.6	0.974

Where: S_{BET} = BET surface area; C_{BET} = BET constant; d_p = pore diameter at the distribution peak; V_p = total volume of pores.

by analyzing Figures 4 to 6, which show the impacts of variations in the silicate modulus, final pH of the reaction and SiO_2 concentration on both in the analysis of BET surface area and in total pore volume of silica gel. In Figure 4, it is observed that only the final pH of the reaction has a significant effect on the surface area of the silica gel, with a sudden drop in S_{BET} for pH ≥ 6. A similar behavior can be observed in Figure 5 for the average pore diameter, with a sudden increase in d_p for pH ≥ 6 and resulting in a drastic change in morphology, from microporous to mesoporous.

In the case of total pore volume, shown in Figure 6, pH clearly has a major effect, but the silicate modulus and SiO_2 concentration also seem to have a small contribution to the characteristic. Given these results, silica with a larger total pore volume was the one produced with intermediate values of Wr and SiO_2, at the central point.

According to the classical theory of silica polymerization proposed by Iler[40], the small particles formed at the beginning of the process, with sizes smaller than 5 nm, are highly soluble due to their high surface energy, and tend to dissolve and redeposit on larger particles (Ostwald ripening), leading to particle growth. When the reaction is carried out at pH ≥ 6, the depolymerization/polymerization rate is high, so that the particle continues to grow rapidly until it reaches approximately 10 nm in diameter (S_{BET} = 300 m^2/g). On the other hand, when the reaction occurs at pH = 4, the maturation process is very slow, and particle growth becomes negligible after the particle reaches 4 nm (S_{BET} = 750 m^2/g). Furthermore, at pH ≥ 6, the surface is more negatively charged and the repulsion between silica particles is high, leading to a lower aggregation rate and resulting in the formation of aggregates with longer branches and greater pore volume. On the contrary, at pH = 4, the surface of the silica particles is poorly charged, leading to a high rate of aggregation, and resulting in the formation of more compact aggregates, with smaller pore volumes[40].

In the hygroscopic regime, the adsorbent capacity of a porous solid is the result of the combination of two factors: the interaction potentials and the morphology of the adsorbent. The phenomenon of adsorption occurs when the potential energy of interaction between adsorbate and adsorbent, φ, equals the work that needs to be done to take a molecule from the gaseous state to the adsorbed state. The total adsorbate-adsorbent interaction energy comprises the contributions of the dispersive, φ_d, and specific, φ_s components. The dispersive component involves van der Waals forces, while the specific component may involve permanent electrical monopoles or multipoles, hydrogen bonds, acid-base interactions, etc[41]. In the case of silicas, specific interactions are preponderant, and therefore the degree of surface hydroxylation of silica is an important physicochemical characteristic for the adsorption phenomenon, as surface silanol groups can interact with water molecules and other molecules polarized by hydrogen bonds[42].

The BET constant, obtained from the BET method for determining surface area, reflects the material's surface adsorption energy and can be used as an approximate measure of the relative proportion of surface siloxane and silanol groups. Thus, the lower the C_{BET} value, the lower the degree of the silica's surface hydroxylation and its capacity to adsorb moisture should be[43]. The effect of varying reaction conditions on C_{BET} is shown in Figure 7. It is observed that the silicate modulus does not appear to have affected C_{BET} significantly, but it is quite evident that, at lower pH and [SiO_2], the silica synthesized showed a lower degree of surface hydroxylation. According to Legrand et al.[44], silanol groups are formed during the synthesis of silica, due to the process of condensation of silicic acid on the surface, and the degree of surface hydroxylation is strongly dependent on the preparation method. However, the literature researched does not indicate a clear relationship between the synthesis parameters and this characteristic. The hypothesis considered to explain the phenomenon is that at low pH the central silicon atoms become more electrophilic due to the electronic drainage suffered, becoming more susceptible to attack by silanol groups (condensation). Consequently, acid catalysis favors the formation of more linear chains (lower number of hydroxylated ends), while basic catalysis leads to more highly branched network structures (higher number of hydroxylated ends), since reactions in terminal silicon atoms are favored[45]. In addition, it can be expected that for lower silicate concentrations the polycondensation kinetics are controlled by diffusion, so that the surface silanols have enough time to react with each other before condensing with new silicic acid molecules, increasing the proportion of siloxane bridges on the surface.

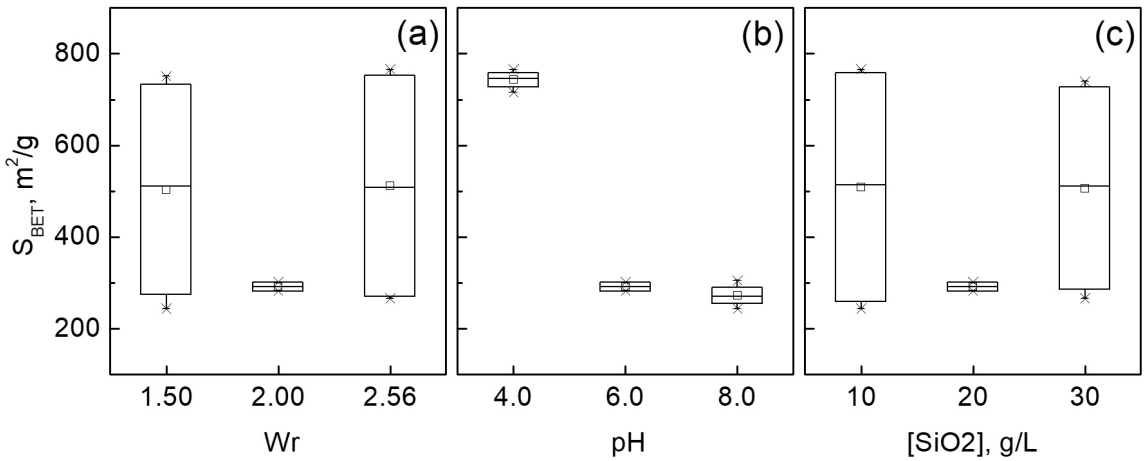

Figure 4. Effects of variations in the silicate modulus (a), final pH of the reaction (b) and SiO_2 concentration (c) on the BET surface area (S_{BET}) of the silica gel.

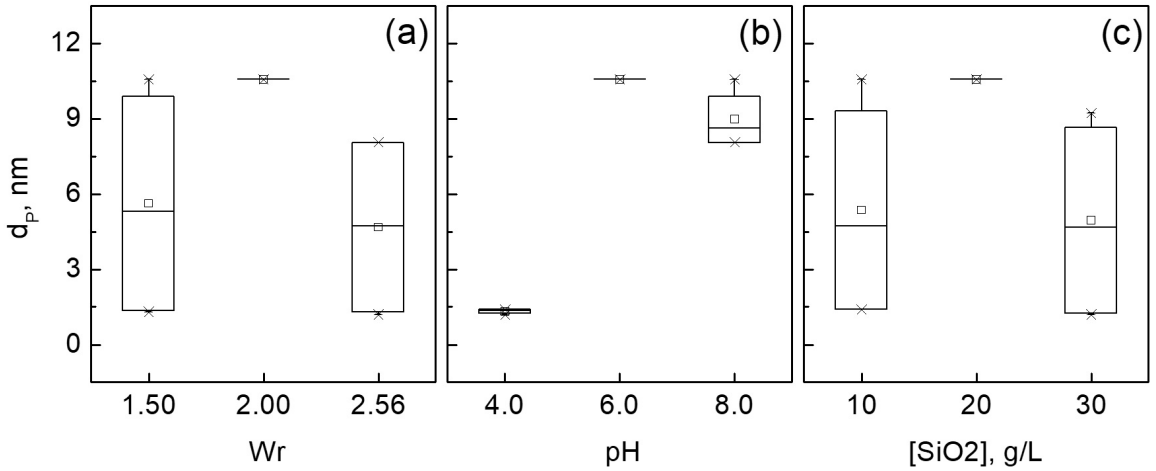

Figure 5. Effects of variations in the silicate modulus (a), final pH of the reaction (b) and SiO_2 concentration (c) on the average pore diameter (d_p) of the silica gel.

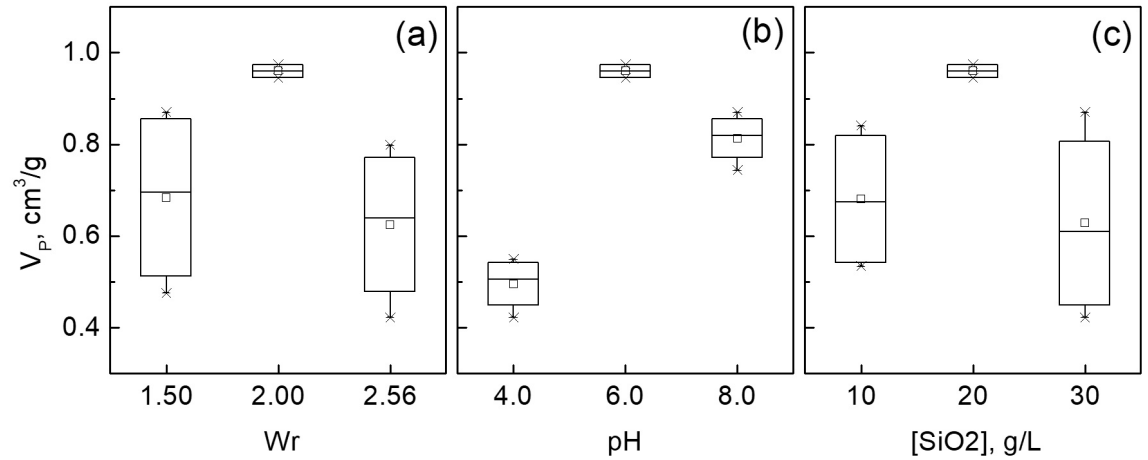

Figure 6. Effects of variations in the silicate modulus (a), final reaction pH (b) and SiO_2 concentration (c) on the total volume of pores (V_p) of the silica gel.

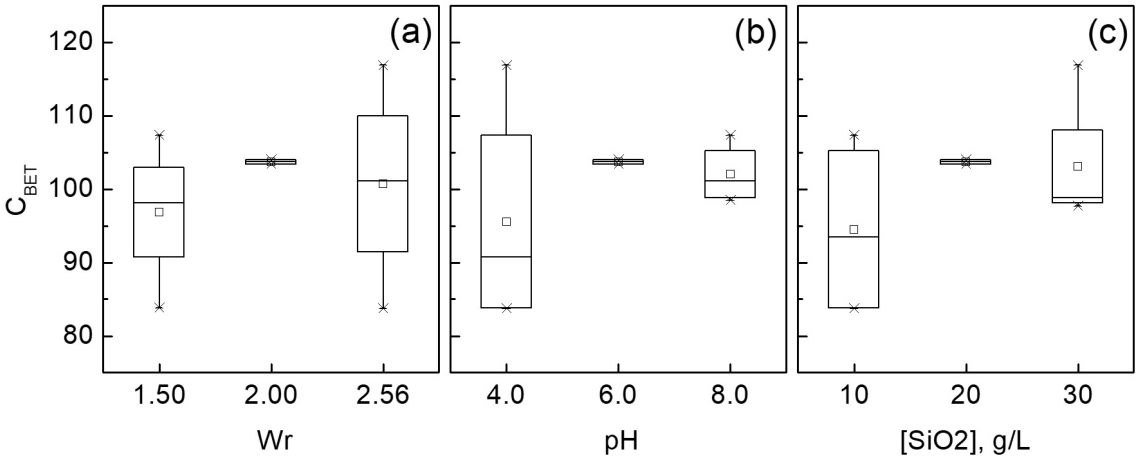

Figure 7. Effects of variations in the silicate modulus (a), final pH of the reaction (b) and SiO2 concentration (c) on the BET constant (C_{BET}) of silica gel.

3.3. Liquid absorption capacity of silica gel

Figures 8 and 9 show the absorption properties of liquid water and simulated body fluid by the different synthesized silicas. It was observed that the degree of absorption was directly proportional to the average size and total volume of the material's pores, and inversely proportional to the surface area. Furthermore, no correlation was observed between liquid absorption capacity and C_{BET}, indicating that the degree of surface hydroxylation does not affect this property significantly.

The observed behavior is opposite to what would be expected for the water adsorption in the vapor phase by silica gels commonly used as desiccants[17,46], which confirms that the ability to absorb liquids is strongly related to the presence of large structural "voids", and less dependent on the surface activity of the silica. Therefore, the mesoporous silica group (R1, R5, R6, R8 and CP) exhibited greater liquid absorption than the microporous silica group (R2, R3, R4 and R7).

3.4. Evaluation of the effect of silica functionalization with ZnO, Ag and Cu on morphological characteristics and liquid absorption

The exuded liquid from fresh meat products during their storage tends to increase the free water availability for oxidation and rancidity reactions, making its removal essential to extend the food's storage time[3]. As observed in the results above, due to the greater capacity to absorb water and simulated body fluid, the silica gel sample identified as "CP" was chosen to be used as matrix for doping with metallic nanoparticles with proven antimicrobial activity[29,31]. In this context, Table 4 shows the morphological characteristics determined by BET, the liquid absorption properties of the silica gel functionalized with metallic nanoparticles obtained, and the amount (nominal) of Cu, Ag and ZnO nanoparticles.

It is observed that the chemical modification resulted in an average reduction of 14% in the surface area and an increase of 5 to 9% in the total pore volume of the functionalized silicas in relation to the CP matrix. This change can be attributed, theoretically, to the partial digestion of the structures during alkali treatment, which favors the Ostwald maturation process[39]. In part, the increase observed in the functionalized silica gels' pore volume in relation to the CP matrix may explain the observed increase in water and SBF absorptions, however, the ZnO-Silica sample presented a superior water absorption and SBF in comparison to the other samples. In order to further investigate this behavior, two more silicas functionalized with ZnO were prepared, with nominal dopant levels of 81 mg/kg and 407 mg/kg, and new water absorption tests were carried out. The results of these water absorption tests for ZnO-functionalized silicas with varying ZnO contents are shown in Figure 10.

From the intersection of the trend line with the y axis in Figure 10, a water absorption value of 215% is obtained, indicating that the increase in pore volume could be responsible for only 11% increase in water absorption capacity (the absorption of the PC sample was 194%), which would also be consistent with the absorption trend shown by the mesoporous samples in Figure 8a. Therefore, the results obtained indicate that the observed excess absorption may be related to the presence of ZnO particles introduced into the silica matrix. According to Li et al.[47], the water absorption capacity of functionalized silica also depends on the polarizability of the metallic particles supported in the matrix. Thus, the greater the polarizability of the doping material, the stronger the attractive forces between the nanoparticle and water, which can result in a greater capacity for liquid retention by the material.

Figure 11 shows the micrographs obtained by TEM for silicas functionalized with Cu-Silica (a, b), Ag-Silica (c, d) and Zn-Silica (e, f) obtained at different magnifications. It was observed that all nanoparticles had an approximately spherical shape, with Ag and ZnO nanoparticles having sizes of up to 15 nm, while Cu nanoparticles had a larger size, up to 30 nm, but within the range considered to have high antimicrobial activity[48]. Furthermore, all identified metallic nanoparticles are apparently anchored in the matrix, with no isolated particles identified. The enhanced antimicrobial effectiveness of nanoparticles and nanofilms, compared to

Table 4. Morphological characteristics and liquid absorption properties of silicas functionalized with Cu, Ag and ZnO nanoparticles.

Sample	Content of added metal	Adsorption N_2 at 77 K		Liquid absorption	
		S_{BET}	V_p	water	SBF
	mg/kg	m^2/g	cm^3/g	%	%
Silica "CP"	—	292	0.960	194	187
Cu-Silica	64	252	1.047	209	221
Ag-Silica	108	259	1.045	204	209
ZnO-Silica	814	245	1.011	245	244

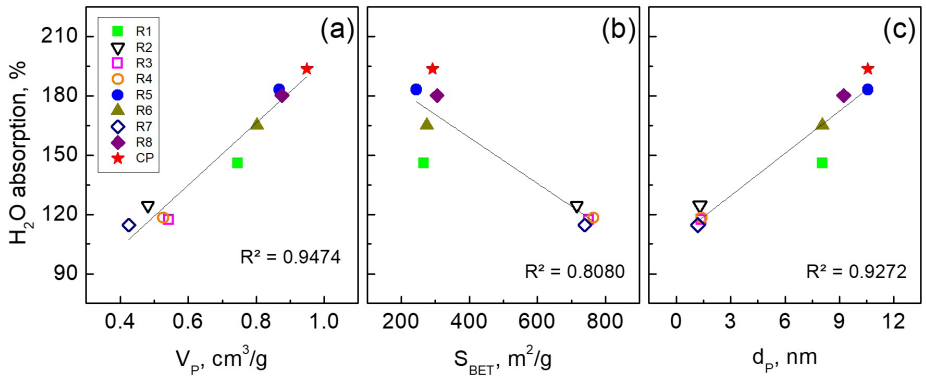

Figure 8. Influence of total pore volume (a), surface area (b) and average pore diameter (c) on the water absorption capacity of silica gel.

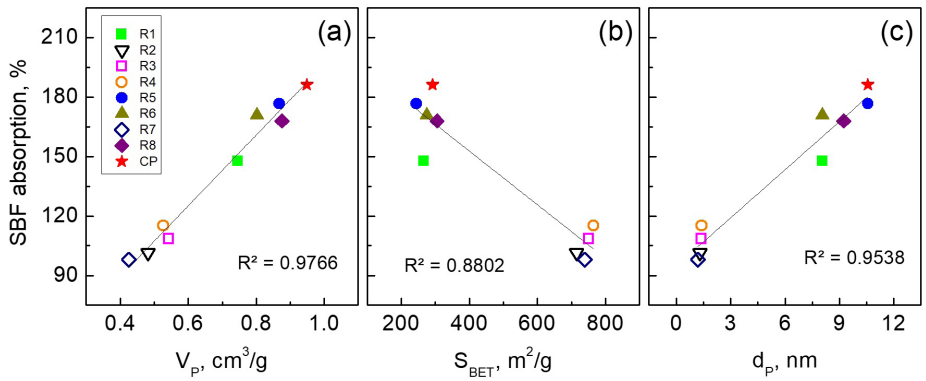

Figure 9. Influence of total pore volume (a), surface area (b) and average pore diameter (c) on the simulated body fluid (SBF) absorption capacity of silica gel.

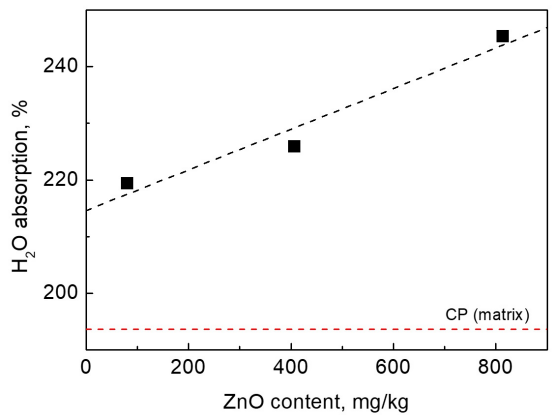

Figure 10. Effect of ZnO nanoparticle content on the water absorption capacity of functionalized silica gel. The absorption capacity of the silica gel identified as CP, used as a matrix for the synthesis of silica functionalized with ZnO, is indicated as a reference in the red dashed line.

materials with micrometric-scale compositions, is attributed to the increased surface area available for interactions with microorganisms. Since the migration of these agents into food is undesirable, the strategy of anchoring the nanoparticles in a matrix, such as silica, is normally adopted[49].

The silica gel functionalized with Ag and ZnO nanoparticles were also tested as absorbent pads in active packaging for meat products and the results were presented in a separate publication[50]. The antimicrobial activity of these nanocomposites through agar diffusion tests was studied, as well as its effectiveness in application in a prototype packaging.

4. Conclusion

This work demonstrated the influence of the synthesis of silica gel and its functionalization with metallic nanoparticles on the liquid absorption capacity, in order to preliminarily evaluate the potential use of these nanocomposites in absorbent pads for active packaging.

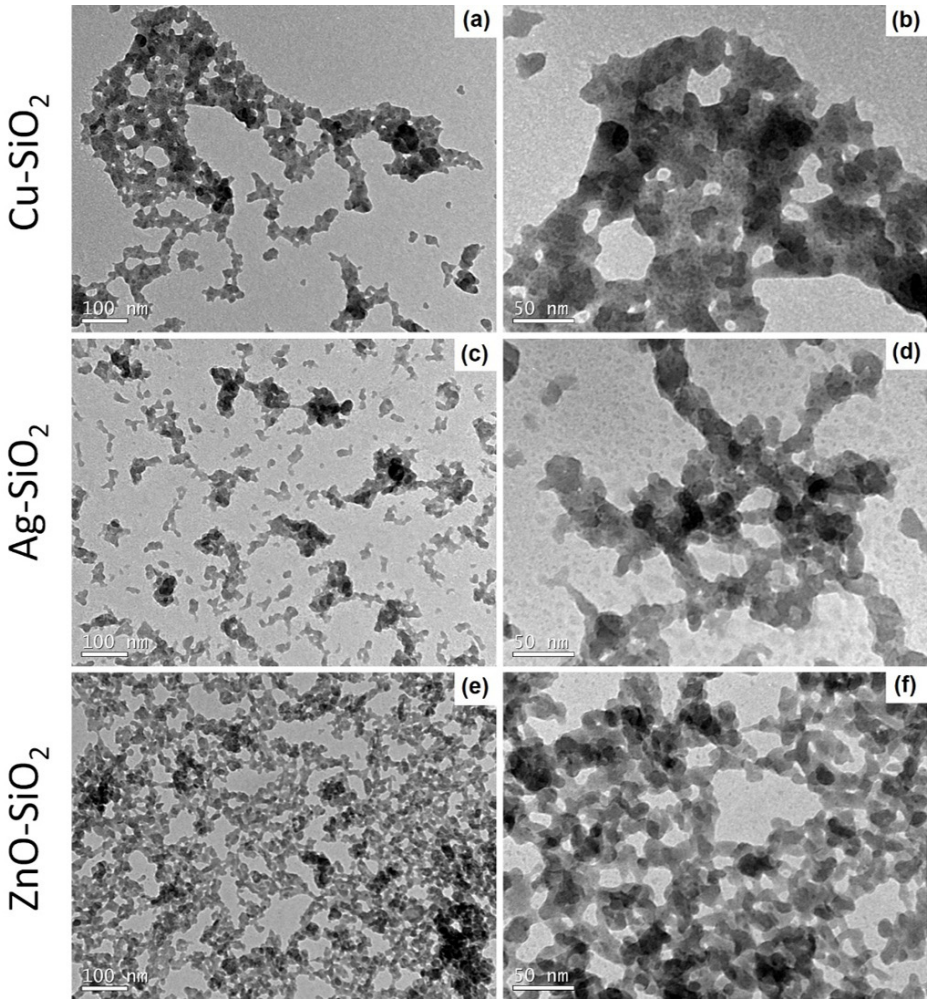

Figure 11. TEM micrographs obtained for the functionalized silicas Cu-SiO_2 (a, b), Ag-SiO_2 (c, d) and Zn-SiO_2 (e, f).

The silica gel was synthesized from sodium silicate obtained from rice husks, a circular and renewable material with a lower carbon footprint than traditional materials currently applied for this purpose. By varying the silica gel synthesis parameters explored by 2×3 factorial design (DOE), it was possible to obtain silicas with varied surface areas (250 – 750 m^2/g) and pore volume (0.4 – 1.0 cm^3/g). The water and simulated body fluid absorption tests indicate that the absorption capacity of these liquids is influenced mainly by the size and volume of silica pores (directly proportional), with no apparent contribution from surface activity. This behavior contrasts with what could be expected for the water adsorption in the vapor state. The sample that showed the greatest effectiveness in absorbing liquids was the CP sample, and thus it was used as a base for functionalization with metallic nanoparticles.

Nanoparticles of Ag, Cu and ZnO were successfully incorporated into the silica gel matrix. The Ag and ZnO nanoparticles presented sizes of up to 15 nm, while the Cu nanoparticles presented a larger size, up to 30 nm, within the range considered to have high antimicrobial activity. The presence of ZnO nanoparticles in silica appears to have contributed, effectively and proportionally to their content, to the absorption of water and simulated body fluid. The antimicrobial activity of these nanocomposites was studied, and the results were presented in a separate publication.

5. Acknowledgments

The authors would like to thank the company Oryzasil Sílicas Naturais for kindly providing the RHA and silicate samples, to CAPES for granting the research grant, and FAPESC (TO 021TR001860).

6. References

1. Brasil. Companhia Nacional de Abastecimento. Acompanhamento da safra brasileira de grãos: safra 2021/22, n.9 - Nono levantamento [Internet]. Brasília: CONAB; 2022 [cited 2024 Sept 30]. Available from: https://www.conab.gov.br/info-agro/safras/graos/boletim-da-safra-de-graos?start=20
2. Fundação Estadual de Proteção Ambiental. Diretriz técnica nº 002/2011. Gestão de resíduos caracterizados como casca de arroz e cinzas resultantes do processo de queima da casca [Internet]. Porto Alegre: FEPAM; 2011 [cited 2024 Sept 30].

Available from: https://ww3.fepam.rs.gov.br/central/diretrizes/Diret_Tec_02_2011.pdf
3. Braga LR, Silva FM. Embalagens ativas: uma nova abordagem para embalagens alimentícias. Braz J Food Res. 2017;8(4):170-86. http://doi.org/10.3895/rebrapa.v8n4.4602.
4. Wang F, Xu Z, Chen L, Qiao Z, Hu Y, Fan X, et al. Super absorbent resilience antibacterial aerogel with curcumin for fresh pork preservation. Food Control. 2024;159:110289. http://doi.org/10.1016/j.foodcont.2024.110289.
5. Yildirim S, Röcker B, Pettersen MK, Nilsen-Nygaard J, Ayhan Z, Rutkaite R, et al. Active packaging applications for food. Compr Rev Food Sci Food Saf. 2018;17(1):165-99. http://doi.org/10.1111/1541-4337.12322.
6. Otoni CG, Espitia PJP, Avena-Bustillos RJ, McHugh TH. Trends in antimicrobial food packaging systems: emitting sachets and absorbent pads. Food Res Int. 2016;83:60-73. http://doi.org/10.1016/j.foodres.2016.02.018.
7. Jiao X, Xie J, Du H, Bian X, Wang C, Zhou L, et al. Antibacterial smart absorbent pad with Janus structure for meat preservation. Food Packag Shelf Life. 2023;37:101066. http://doi.org/10.1016/j.fpsl.2023.101066.
8. Wang F, Xu Z, Chen L, Qiao Z, Hu Y, Fan X, et al. Super absorbent resilience antibacterial aerogel with curcumin for fresh pork preservation. Food Control. 2024;159:110289. http://doi.org/10.1016/j.foodcont.2024.110289.
9. Dong H, Xu Y, Zhang Q, Li H, Chen L. Activity and safety evaluation of natural preservatives. Food Res Int. 2024;190:114548. http://doi.org/10.1016/j.foodres.2024.114548.
10. Lan W, Zhang R, Ahmed S, Qin W, Liu Y. Effects of various antimicrobial polyvinyl alcohol/tea polyphenol composite films on the shelf life of packaged strawberries. Lebensm Wiss Technol. 2019;113:108297. http://doi.org/10.1016/j.lwt.2019.108297.
11. Ju J, Chen X, Xie Y, Yu H, Guo Y, Cheng Y, et al. Application of essential oil as a sustained release preparation in food packaging. Trends Food Sci Technol. 2019;92:22-32. http://doi.org/10.1016/j.tifs.2019.08.005.
12. Dey A, Pandey G, Rawtani D. Functionalized nanomaterials driven antimicrobial food packaging: A technological advancement in food science. Food Control. 2022;131:108469. http://doi.org/10.1016/j.foodcont.2021.108469.
13. Schaller J, Cramer A, Carminati A, Zarebanadkouki M. Biogenic amorphous silica as main driver for plant available water in soils. Nat Res. 2020;10(1):1-7. http://doi.org/10.15495/EPub_UBT_00005381.
14. Wilson CT, Harte J, Almenar E. Effects of sachet presence on consumer product perception and active packaging acceptability: a study of fresh-cut cantaloupe. Lebensm Wiss Technol. 2018;92:531-9. http://doi.org/10.1016/j.lwt.2018.02.060.
15. Murmu SB, Mishra HN. Selection of the best active modified atmosphere packaging with ethylene and moisture scavengers to maintain quality of guava during low temperature storage. Food Chem. 2018;253:55-62. http://doi.org/10.1016/j.foodchem.2018.01.134.
16. Li F, Lei C, Shen Q, Li L, Wang M, Guo M, et al. Analysis of copper nanoparticles toxicity based on a stress-responsive bacterial biosensor array. Nanoscale. 2013;5(2):653-62. http://doi.org/10.1039/C2NR32156D.
17. Zheng X, Ge TS, Wang RZ, Hu LM. Performance study of composite silica gels with different pore sizes and different impregnating hygroscopic salts. Chem Eng Sci. 2014;120:1-9. http://doi.org/10.1016/j.ces.2014.08.047.
18. Fernandez A, Picouet PA, Lloret E. Reduction of the spoilage-related microflora in absorbent pads by silver nanotechnology during modified atmosphere packaging of beef meat. J Food Prot. 2010;73(12):2263-9. http://doi.org/10.4315/0362-028X-73.12.2263.
19. Capelezzo AP, Mohr LC, Dalcanton F, Barreta CRDM, Martins MAPM, Fiori MA, et al. Polímero biodegradável antimicrobiano através da aditivação com compostos à base de zinco. Quim Nova. 2018;41(4):367-74. http://doi.org/10.21577/0100-4042.20170187.
20. Braga LR, Peres L. Novas tendências em embalagens para alimentos: revisão. Bol Cent Pesqui Process Aliment. 2010;28(1):69-84. http://doi.org/10.5380/cep.v28i1.17899.
21. Gogotsi YG, Uvarova IV, editors. Nanostructured materials and coatings for biomedical and sensor applications. Dordrecht: Springer; 2003. http://doi.org/10.1007/978-94-010-0157-1.
22. Buitrago-Tello R, Venditti RA, Jameel H, Yao Y, Echeverria D. Carbon footprint of bleached softwood fluff pulp: detailed process simulation and environmental life cycle assessment to understand carbon emissions. ACS Sustain Chem& Eng. 2022;10(28):9029-40. http://doi.org/10.1021/acssuschemeng.2c00840.
23. Kokubo T, Takadama H. How useful is SBF in predicting in vivo bone bioactivity? Biomaterials. 2006;27(15):2907-15. http://doi.org/10.1016/j.biomaterials.2006.01.017.
24. ISO: International Organization for Standardization. ISO 1690: sodium and potassium silicates for industrial use: determination of silica content: gravimetric method by insolubilization. Geneva: ISO; 1976.
25. ISO: International Organization for Standardization. ISO 1692: sodium and potassium silicates for industrial use: determination of total alkalinity: titrimetric method. Geneva: ISO; 1976.
26. Besbes M, Fakhfakh N, Benzina M. Characterization of silica gel prepared by using sol-gel process. Phys Procedia. 2009;2(3):1087-95. http://doi.org/10.1016/j.phpro.2009.11.067.
27. Sdiri A, Higashi T, Bouaziz S, Benzina M. Synthesis and characterization of silica gel from siliceous sands of southern Tunisia. Arab J Chem. 2014;7(4):486-93. http://doi.org/10.1016/j.arabjc.2010.11.007.
28. Aimjaijit W, Chaiwiwatworakul P, Chuangchote S. Synthesis of silica gel and development of coating method for applications in a regenerative air dehumidifier. Appl Mech Mater. 2016;839:70-4. http://doi.org/10.4028/www.scientific.net/AMM.839.70.
29. Safavinia L, Akhgar MR, Tahamipour B, Ahmadi SA. Green synthesis of highly dispersed zinc oxide nanoparticles supported on silica gel matrix by daphne oleoides extract and their antibacterial activity. Iran J Biotechnol. 2021;19(1):86-95. http://doi.org/10.30498/ijb.2021.2598.
30. Thanh Hai NT, Phuong TNM, Luong NV, Toan DK, Hoa TT, Thuy NTT. Synthesis and in vitro antifungal efficacy of copper-silica nanocomposites against pathogenic fungi of rice. Tu Nhien Va Cong Nghe. 2020;36(4):51-61. http://doi.org/10.25073/2588-1140/vnunst.5056.
31. Peszke J, Dulski M, Nowak A, Balin K, Zubko M, Sulowicz S, et al. Unique properties of silver and copper silica-based nanocomposites as antimicrobial agents. RSC Advances. 2017;7(45):28092-104. http://doi.org/10.1039/C7RA00720E.
32. Dulski M, Peszke J, Wlodarczyk J, Sulowicz S, Piotrowska-Seget Z, Dudek K, et al. Physicochemical and structural features of heat-treated silver-silica nanocomposite and their impact on biological properties. Mater Sci Eng C. 2019;103:109790. http://doi.org/10.1016/j.msec.2019.109790.
33. Brunauer S, Emmett PH, Teller E. Adsorption of gases in multimolecular layers. J Am Chem Soc. 1938;60(2):309-19. http://doi.org/10.1021/ja01269a023.
34. Barrett EP, Joyner LG, Halenda PP. The determination of pore volume and area distributions in porous substances. I. Computations from nitrogen isotherms. J Am Chem Soc. 1951;73(1):373-80. http://doi.org/10.1021/ja01145a126.
35. Mikhail RSH, Brunauer S, Bodor EE. Investigations of a complete pore structure analysis. J Colloid Interface Sci. 1968;26(1):45-53. http://doi.org/10.1016/0021-9797(68)90270-1.
36. Schaller J, Cramer A, Carminati A, Zarebanadkouki M. Biogenic amorphous silica as main driver for plant available water in soils. Sci Rep. 2020;10(1):2424. http://doi.org/10.1038/s41598-020-59437-x.

37. Thommes M, Kaneko K, Neimark A, Olivier JP, Rodriguez-Reinoso F, Rouquerol J, et al. Physisorption of gases, with special reference to the evaluation of surface area and pore size distribution (IUPAC Technical Report). Pure Appl Chem. 2015;87(9-10):1051-69. http://doi.org/10.1515/pac-2014-1117.
38. Rouquerol F, Rouquerol J, Llewellyn P, Sing KSW, Maurin G, editors. Adsorption by powders and porous solids: principles, methodology and applications. Cambridge: Academic Press; 2014.
39. Vansant EF, van der Voort P, Vrancken KC, editors. Characterization and chemical modification of the silica surface. Amsterdam: Elsevier; 1995.
40. Iler RK, editor. The chemistry of silica: solubility, polymerization, colloid and surface properties and biochemistry of silica. Hoboken: Wiley-Interscience; 1979.
41. Yang RT. Adsorbents: fundamentals and applications. Hoboken: John Wiley & Sons; 2003. http://doi.org/10.1002/047144409X.
42. Christy AA. The nature of silanol groups on the surfaces of silica, modified silica and some silica based materials. Adv Mat Res. 2014;998-999:3-10. http://doi.org/10.4028/www.scientific.net/AMR.998-999.3.
43. Lowen WK, Broge EC. Effect of dehydratation and chemisorbed materials on the surface properties of amorphous silica. J Phys Chem. 1961;65(1):16-9. http://doi.org/10.1021/j100819a006.
44. Legrand AP, Hommel H, Tuel A, Vidal A, Balard H, Papirer E, et al. Hydroxyls of silica powders. Adv Colloid Interface Sci. 1990;33(2-4):91-330. http://doi.org/10.1016/0001-8686(90)80027-W.
45. Levy D, Zayat M, editors. The sol-gel handbook, 3 volume set: synthesis, characterization, and applications. Hoboken: John Wiley & Sons; 2015. http://doi.org/10.1002/9783527670819.
46. Bu X, Wang L, Huang Y. Effect of pore size on the performance of composite adsorbent. Adsorption. 2013;19(5):929-35. http://doi.org/10.1007/s10450-013-9513-8.
47. Li X, Li H, Huo S, Li Z. Dynamics and isotherms of water vapor sorption on mesoporous silica gels modified by different salts. Kinet Catal. 2010;51(5):754-61. http://doi.org/10.1134/S0023158410050186.
48. Lai MJ, Huang YW, Chen HC, Tsao LI, Chien CFC, Singh B, et al. Effect of size and concentration of copper nanoparticles on the antimicrobial activity in *Escherichia coli* through multiple mechanisms. Nanomaterials. 2022;12(21):3715. http://doi.org/10.3390/nano12213715.
49. Radusin TI, Ristić IS, Pilić BM, Novaković AR. Antimicrobial nanomaterials for food packaging applications. Food Feed Res. 2016;43(2):119-26. http://doi.org/10.5937/FFR1602119R.
50. Guido ZNS, Braum MV, Possolli NM, De Bonna R, Ponsoni LV, de Almeida MK, et al. Part 2: the effect of functionalizing silica gel with Ag and ZnO nanoparticles on antimicrobial properties and their application in meat packaging. SSRN. 2024. http://doi.org/10.2139/ssrn.4956871.